Periodically driven facilitated high-efficiency dissipative entanglement with Rydberg atoms

Rui Li,[1] Dongmin Yu,[1] Shi-Lei Su,[2,*] and Jing Qian[1,†]

[1]*State Key Laboratory of Precision Spectroscopy, Quantum Institute for Light and Atoms, Department of Physics, School of Physics and Electronic Science, East China Normal University, Shanghai 200062, China*

[2]*School of Physics, Zhengzhou University, Zhengzhou 450001, China*

(Received 24 October 2019; revised manuscript received 11 March 2020; accepted 17 March 2020; published 23 April 2020)

A time-dependent periodical field can be utilized to efficiently modify the Rabi coupling of system, exhibiting nontrivial dynamics. We propose a scheme to show that this feature can be utilized for speeding up the formation of dissipative steady entanglement based on the Rydberg antiblockade mechanism. When the modulation frequency is exactly equal to the central frequency of the driving field, a sufficient residence time of the two-excitation Rydberg state is allowed for an irreversible spontaneous decay onto the target state, leading to a steady entanglement with a high fidelity $\sim$0.98 and a shorter generation time $<$400 μs. We show that a global maximal fidelity benefits from a consistence of microwave-field coupling and spontaneous decay strengths. The scheme manifests robust insensitivities towards the imperfect initialization, the fluctuations of van der Waals interaction, and the modulation frequency. This simple approach to facilitate the generation of dissipative entangled two-qubit states may guide an experimental direction in Rydberg quantum technology and quantum information.

DOI: 10.1103/PhysRevA.101.042328

I. INTRODUCTION

Dissipative mechanism, in contrast to its natural idea that leads to the destruction of quantum effects de-coherently, can counterintuitively serve as an important resource for implementing quantum information task and controlled quantum state preparation [1–8]. Experimental achievements towards dissipative production of entangled states have been implemented in trapped ions [9,10], superconducting quantum bits [11,12], and macroscopic atomic ensembles [13].

It is remarkable that pioneer works demonstrating preparation of dissipative steady entanglement from an uppermost Rydberg level were proposed by Saffman [14] and Mølmer [15], providing great potentials for applications of quantum computation and engineering by Rydberg dissipation [16,17]. However, a typical period needed for this dissipative preparation exceeded hundreds of milliseconds due to the use of a high-lying long-lived Rydberg level with principle quantum number $n \sim 125$; e.g., see [18,19]. So far great efforts are devoted to accelerate the formation of an entangled steady state by the method of Rydberg electromagnetically induced transparency [15]. In the method a fast-decaying middle state in the presence of Rydberg interactions permits a rapid entangled-state generation. Nevertheless, this approach still has not been realized in experiment due to the complexity of coupling strategy of laser fields and energy levels [20–22].

Other alternative approaches are proposed by employing an optical cavity to trigger the entanglement formation, because the cavity decay treating as an auxiliary loss channel towards the target state can permit a reduced stabilization time which is smaller than tens of microseconds [23–27]. More recently an intriguing improvement for realizing a ten-times faster generation of entanglement was reported in the cavity, arising an exponential enhancement for the atom-cavity coupling strength [22]. Nevertheless these schemes based on cavity-trapped atoms require a stronger atom-cavity coupling associated with a precise control, which remains uneasy for real implementations.

In parallel, periodically driven systems are well known in quantum physics arising a wealth of versatile quantum phenomena [28–31]. For example, the simplest two-level atom system having a periodically modulated driving can significantly modify the time evolution of the system [32,33]. That fact has raised intriguing effects including persistent atomic trapping in excited state [34], an excited two-level emitter [35], multiphoton resonance and response [36], maximal population transfer [29], discrete time crystals [37,38], and so on. In addition, periodically driven dissipative (open) systems offer various prospects for the new-class feature of out-of-equilibrium physics which are inaccessible for equilibrium ensembles [39–41], covering promising applications from topological states to experimental optomechanics [42–45]. Besides combining periodically driven with a Rydberg atom array is found to produce the localization of a quantum many-body state [46]. And, more recently, a mechanism relying on an amplitude-modulated periodic field is exploited for generating dissipative steady-state entanglement in a solid-state qubit system [47], bringing more perspectives for nontrivial periodically driven Rydberg features.

In the present work, we develop a simplified scheme for speeding up the dissipative preparation of a maximal steady entangled state $|S\rangle = \frac{1}{\sqrt{2}}(|10\rangle - |01\rangle)$, essentially based on a

*slsu@zzu.edu.cn

†Corresponding author: jqian1982@gmail.com

periodic pump driving as well as the Rydberg antiblockade mechanism. Remarkably, if an external modulation frequency is consistent with the characteristic frequency of the effective two-state system, it will arise to a significant change to the Rabi behavior of the two-excitation Rydberg state in the laser pumping process, which benefits from a fast decaying onto the target state due to a longer residence time. Accompanied by a suitable adjustment for other dissipative rate and microwave coupling strength, the resulting entanglement formation reveals a stepwise acceleration towards the target entangled state acquiring a very high fidelity ∼0.98, where the required convergence time can be shorter than ∼400 μs. Because a stepwise-improving entangled-state accumulation rate will appear within these durations, in contrast to the case of a continuous driving in which the rate of population accumulation persists slowly. Additionally we demonstrate an easy way for further acceleration by increasing the effective Rabi coupling strength in the pumping, and stress the robust insensitivities of the scheme to arbitrary initial preparation, variable interaction, and driving frequency under real experimental parameters.

II. THEORETICAL FORMULATION

A. Single original four-level atom

To verify the validity of our effective five-level scheme as adopted in Fig. 2(b), we first begin with an original four-level atom with ground state $|1\rangle$, middle state $|p\rangle$, and Rydberg state $|r\rangle$ composing a two-photon excitation [48], where the Rabi frequencies are denoted by Ω_p and $\Omega_s(t)$ (time dependent) and the corresponding detunings are Δ_1 and Δ_2. State $|0\rangle$ serves as an auxiliary ground state introduced to achieve a weak microwave coupling g with state $|1\rangle$. Alternatively, this could also be accomplished with a Raman process with respect to $|p\rangle$; e.g., see Fig. 1(c).

Converting into the interaction picture, the Hamiltonian of the single atom reads as $\hat{\mathcal{H}}_1 = \hat{\mathcal{H}}_{1d} + g/2(|1\rangle\langle 0| + |0\rangle\langle 1|)$ with the atom-light interaction term $\hat{\mathcal{H}}_{1d}$ taking the form of

$$\hat{\mathcal{H}}_{1d} = \frac{\Omega_p}{2} e^{-i\Delta_1 t}|p\rangle\langle 1| + \frac{\Omega_s(t)}{2} e^{-i\Delta_2 t}|r\rangle\langle p| + \text{H.c.} \quad (1)$$

By assuming the condition of two-photon resonance $\Delta_1 + \Delta_2 = 0$ by $\delta = |\Delta_{1,2}|$, if a big detuning to $|p\rangle$ is used by satisfying $\delta \gg \Omega_p, \Omega_s(t)$, it is reasonable to eliminate state $|p\rangle$ in an adiabatic way [49], leading to a direct coupling between $|1\rangle$ and $|r\rangle$. Then the Hamiltonian $\hat{\mathcal{H}}_{1d}$ is modified to be

$$\hat{\mathcal{H}}'_{1d} = \frac{\Omega_p^2}{4\delta}|1\rangle\langle 1| + \frac{\Omega_s^2(t)}{4\delta}|r\rangle\langle r| + \frac{\Omega_p\Omega_s(t)}{4\delta}(|r\rangle\langle 1| + |1\rangle\langle r|). \quad (2)$$

After some organization the entire single-atom Hamiltonian $\hat{\mathcal{H}}_1$ can be rewritten in a reduced form only referring to states $\{|1\rangle, |r\rangle, |0\rangle\}$, as

$$\hat{\mathcal{H}}_1 = -\Delta(t)|r\rangle\langle r| + \left(\frac{\Omega(t)}{2}|r\rangle\langle 1| + \frac{g}{2}|1\rangle\langle 0| + \text{H.c.}\right), \quad (3)$$

with the two effective parameters [50]

$$\Omega(t) = \frac{\Omega_p\Omega_s(t)}{2\delta}, \quad \Delta(t) = \frac{\Omega_p^2 - \Omega_s^2(t)}{4\delta},$$

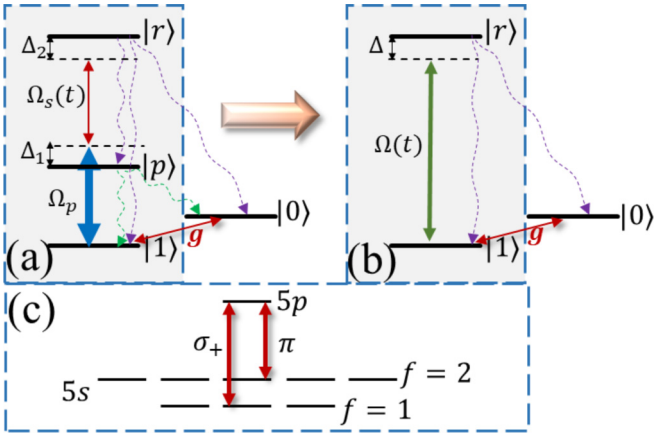

FIG. 1. (a), (b) Schematic of an effective three-level atom deriving from its original form of a four-level configuration. See texts for detailed parameter descriptions. (c) For example, the two hyperfine ground states $|1\rangle = |5s, f = 1, m_f = 0\rangle$, $|0\rangle = |5s, f = 2, m_f = 0\rangle$ are coupled by a weakly resonant Raman coupling with respect to the middle state $|p\rangle = |5p\rangle$, or by a direct microwave coupling g between $|0\rangle$ and $|1\rangle$.

as represented in Fig. 1(b). State $|1\rangle$ is straightforwardly excited to the highly excited level $|r\rangle$ via a time-dependent Rabi frequency $\Omega(t)$, detuned by Δ. Noting if $\Omega_p \gg |\Omega_s(t)|$ the detuning Δ approximately preserves a constant $\Omega_p^2/4\delta$ that does not depend on the time t. The microwave coupling g is too small to affect the strong atom-light interaction, safely leaving it unvaried in Eq. (3). All spontaneous dissipations from $|r\rangle$, $|p\rangle$ are considered, denoted by γ, Γ, respectively. A numerical verification for the correctness of the effective model will be left for discussion in Appendix A, by comparing to the results directly from the original system.

B. Pair of reduced three-level atoms

We proceed to show more essences of energy structure when a pair of effective three-level atoms are involved. The relevant energy levels interested have been represented in Fig. 2(a) composing two reduced three-level Λ interacting atoms [Fig. 1(b)]. For each atom consisting of two ground states $|0\rangle$, $|1\rangle$ and one Rydberg state $|r\rangle$, the hyperfine states $|0\rangle$ and $|1\rangle$ suffering from dipole forbidden are coupled by a microwave field with strength g, which can receive the population from $|r\rangle$ through stochastic spontaneous emission decays by rate γ. Population accumulated on other hyperfine ground states rather than $|0\rangle$ and $|1\rangle$ can be repumped onto $|0\rangle$ or $|1\rangle$ by recycling lasers (not shown) [14]. Special attention is paid to the optical transition between $|1\rangle$ and $|r\rangle$ driven by a time-dependent field $\Omega(t)$, accompanied by a big detuning Δ [assuming $\Delta \gg \Omega(t)/\sqrt{2}$] for realizing a complete suppression to the singly excited collective states. U_{rr} describes the two-atom van der Waals (vdW) -type interaction, making it dynamically compensate the detuning of $|rr\rangle$ by $U_{rr} = 2\Delta$, which can facilitate a direct resonant coupling $\Omega(t)^2/2\Delta$ between $|11\rangle$ and $|rr\rangle$ via adiabatically eliminating the middle single-excitation Rydberg states, as shown in Fig. 2(b).

In a rotating-wave frame, the basic Hamiltonian for a pair of three-level atoms involving the single-atom Hamiltonian

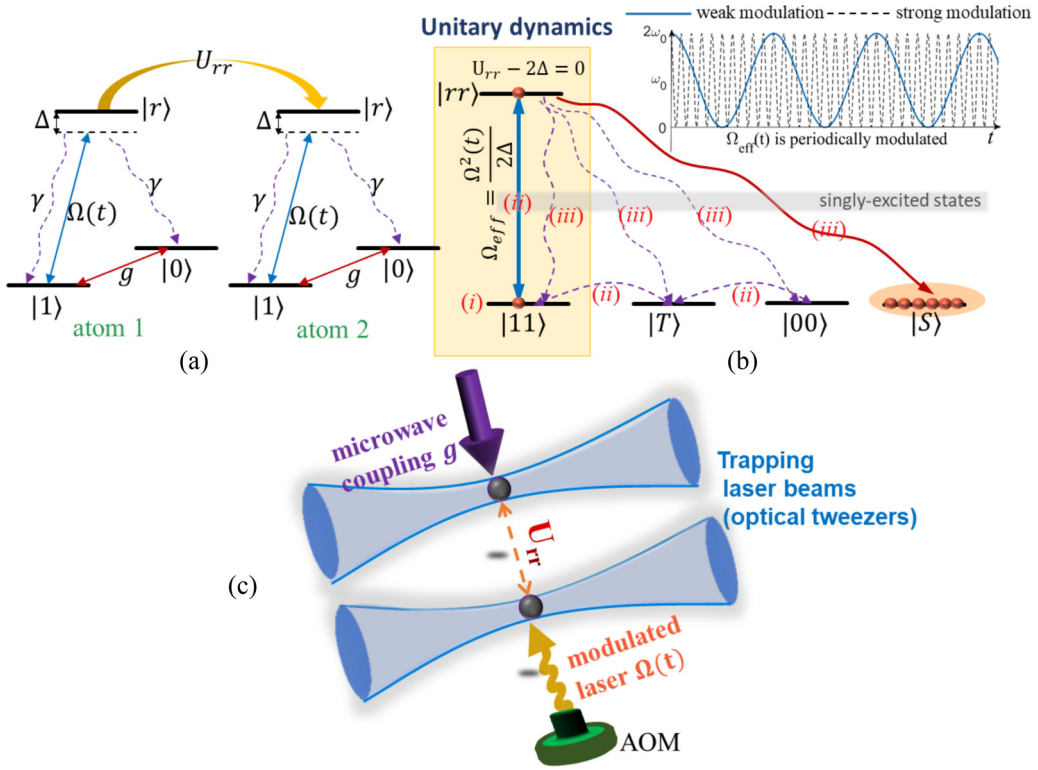

FIG. 2. Schematic diagram of a high-fidelity facilitated entanglement preparation. (a) A detailed two-atom energy-level structure. For each atom, two ground states $|1\rangle$ and $|0\rangle$ are coupled by a continuous microwave field g, and $|1\rangle$ is far-off resonantly coupled to the Rydberg state $|r\rangle$ via a periodically modulated optical field with the Rabi frequency $\Omega(t)$. Assuming that the detuning Δ can compensate the interaction induced energy shift U_{rr} by satisfying the antiblockade condition $U_{rr} = 2\Delta$ persistently, $|11\rangle$ is directly coupled to $|rr\rangle$ via a two-photon excitation with an effective value $\Omega^2(t)/2\Delta$. (b) The effective five-level diagram from a pair of three-level atoms shows the real atom-field interactions and spontaneous decays, where the four singly excited states (gray shadow area) are safely discarded due to $\Delta \gg \Omega(t)/\sqrt{2}$. $|S\rangle$ is a target dark entangled state, unidirectionally receiving the population from $|rr\rangle$ through spontaneous emission. The amplitude of $\Omega_{\rm eff}(t)$ is illustrated in the inset where blue-solid and black-dashed curves stand for weak and strong frequency modulations, respectively. (c) The experimental setup (proposal; see Sec. V for detailed experimental parameters). Two atoms are trapped in dipolar traps formed by tightly focused laser beams (optical tweezers) with interatomic distance R close to the critical value R_c, leading to the strength of van der Waals–type interaction $U_{\rm rr} = C_6/R^6$ between two individual atoms. They are also persistently driven by a microwave field g as well as a periodically modulated optical field $\Omega(t)$, realized by an acousto-optical modulator in the experimental implementation. The variation of interaction $\delta U(t)$ due to the imperfect position confinement in the foci of optical tweezers typically <1 μm will be discussed in Sec. VI B.

$\hat{\mathcal{H}}_1$ reads

$$\hat{\mathcal{H}} = \hat{\mathcal{H}}_1 \otimes \hat{I} + \hat{I} \otimes \hat{\mathcal{H}}_1 + \hat{v}, \tag{4}$$

where $\hat{I}$ is a 3×3 unit operator. $\hat{v}$ describes the two-atom Rydberg interaction given by $\hat{v} = U_{\rm rr}|rr\rangle\langle rr|$.

Using the two-atom base vectors that contain one doubly excited state $|rr\rangle$, four singly excited states $|r1\rangle$, $|1r\rangle$, $|r0\rangle$, $|0r\rangle$, and four ground states $|00\rangle$, $|11\rangle$, $|T\rangle$, $|S\rangle$, the complete decay behavior (dissipation) can be expressed by the regular Lindblad operators,

$$\begin{aligned}
\hat{L}_1 &= \sqrt{\gamma}[|11\rangle\langle r1| + (|T\rangle + |S\rangle)\langle r0| + |1r\rangle\langle rr|], \\
\hat{L}_2 &= \sqrt{\gamma}[|11\rangle\langle 1r| + (|T\rangle - |S\rangle)\langle 0r| + |r1\rangle\langle rr|], \\
\hat{L}_3 &= \sqrt{\gamma}[|00\rangle\langle r0| + (|T\rangle - |S\rangle)\langle r1| + |0r\rangle\langle rr|], \\
\hat{L}_4 &= \sqrt{\gamma}[|00\rangle\langle 0r| + (|T\rangle + |S\rangle)\langle 1r| + |r0\rangle\langle rr|],
\end{aligned} \tag{5}$$

corresponding to the spontaneous decay channels of $|r\rangle \to |1\rangle$ ($\hat{L}_{1,2}$) and of $|r\rangle \to |0\rangle$ ($\hat{L}_{3,4}$), respectively. Note that the ground states $|01\rangle$, $|10\rangle$ have been re-organized into the collective singlet states $|S\rangle = (|10\rangle - |01\rangle)/\sqrt{2}$, $|T\rangle = (|10\rangle + |01\rangle)/\sqrt{2}$, where $|S\rangle$ is a unique dark state, absolutely decoupled from other two-atom ground base vectors by $\langle S|\hat{\mathcal{H}}_1|ij\rangle \equiv 0$ ($ij \in \{T, 00, 11\}$).

Consequently it is reliable to prepare the maximal entangled state $|S\rangle$ through a unidirectional spontaneous loss from the doubly excited state $|rr\rangle$ as shown by a thick red arrow in Fig. 2(b). Here the singly excited states have been safely discarded due to a big detuning Δ with respect to $|r\rangle$; the preparation efficiency for entanglement formation mainly depends on the competition between excitation or deexcitation rates of $|11\rangle \leftrightarrow |rr\rangle$ and the unidirectional decay process ($\propto \gamma$) from $|rr\rangle$ to $|S\rangle$.

Remarkably, in the presence of a periodical modulation to the amplitude of $\Omega(t)$, the Rabi behavior between $|11\rangle$ and $|rr\rangle$ will be significantly changed, producing complex multifrequency oscillations [33]. We verify that the resulting formation of target ground state $|S\rangle$ can be dramatically

accelerated under an optimization for relevant frequency parameters.

C. Effective five-level system

The physical essence for robustly fast preparation based on a simplified five-level scheme [see Fig. 2(b); note that the four singly excited states are adiabatically discarded due to the far-off one-photon resonance] can be understood in three steps.

(i) State initialization. Prepare two atoms in ground states, e.g., $|11\rangle$ (robustness of scheme to arbitrary initial states will be discussed in Sec. VI A).

(ii) Circular unitary dynamics and microwave coupling. A two-state unitary dynamics leads to exchanged population (excitation and deexcitation) by an engineered Rabi oscillation between $|11\rangle$ and $|rr\rangle$, governed by a reduced two-state Hamiltonian

$$\hat{\mathcal{H}}_{\text{eff,uni}} = \Omega_{\text{eff}}(t)(|11\rangle + |rr\rangle)(\langle 11| + \langle rr|), \tag{6}$$

where $\Omega_{\text{eff}}(t) = \Omega(t)^2/2\Delta$. Here the driving field $\Omega(t)$ is time dependent, accompanied by a microwave coupling g persistently transferring population among $|11\rangle$, $|T\rangle$, and $|00\rangle$. Notice that $|11\rangle$ and $|00\rangle$ are indirectly coupled via the state $|T\rangle$. This process can be expressed by Hamiltonian $\hat{\mathcal{H}}_{\text{eff,mw}}$

$$\hat{\mathcal{H}}_{\text{eff,mw}} = \frac{g}{\sqrt{2}}(|11\rangle\langle T| + |T\rangle\langle 00|) + \text{H.c.} \tag{7}$$

(iii) Dissipative formation. Owing to the limited lifetime of $|rr\rangle$, in the effective five-level frame population on $|rr\rangle$ suffers from a big spontaneous loss, randomly decaying into four ground states. Once it possibly decays into the unique dark state $|S\rangle$, population will be irreversibly accumulated on it; otherwise, they repeatedly experience circular steps (ii) $\leftrightarrows$ (iii) by following the route of returning to step (ii) again, until the system is finally stabilized onto state $|S\rangle$.

Shortly concluded, ideally the target entangled state $|S\rangle$ can be deterministically created for a sufficiently long time, robustly insensitive to arbitrary optical and microwave drivings. In fact this time could be endless which is impossible for real experimental measurement during a finite detection time. So achieving a fast and high-fidelity entanglement depending on a simplified and feasible protocol with Rydberg atoms remains challenging, having attracted numerous efforts in theory [20–22,51]. Presently we show another way by implementing a periodical modulation to the amplitude of the pump field, revealing a dramatic facilitation to the circular process between (ii) $\leftrightarrows$ (iii), which finally breaks until the unique entangled state $|S\rangle$ is entirely populated. Our results have verified that the formation time for a high-fidelity steady entanglement can be accelerated by orders of magnitude compared with the case of no modulation.

In addition, a further extension for the entanglement formation between two mesoscopic atomic ensembles can be considered by two Rydberg superatoms that allow for only single collective Rydberg excitation within the blockade radius. In fact, it is more attractive to utilize the dissipation-based method in experiment due to its deterministic implementation, and the first demonstration of dissipative entanglement generation with two ground atomic ensembles has been reported [13]. As for two Rydberg superatoms, the computational basis states of each ensemble can be expressed as [52,53]

$$|G_1\rangle = |1_1, \ldots, 1_N\rangle, \tag{8}$$

$$|G_0\rangle = \frac{1}{\sqrt{N}}\sum_{k=1}^{N}|1_1 1_2, \ldots, 0_k, \ldots, 1_N\rangle, \tag{9}$$

$$|R\rangle = \frac{1}{\sqrt{N}}\sum_{k=1}^{N}|1_1 1_2, \ldots, r_k, \ldots, 1_N\rangle, \tag{10}$$

with two collective ground states $|G_1\rangle$, $|G_0\rangle$ and a collective singly excited state $|R\rangle$ of the Rydberg superatom, formed by strong blockade to prohibit the multiatom excitation in the ensemble. These new basis states are convincible only when the dephasing effect of state coming from atomic motions can be negligible. Luckily as we know a typical relaxation time of atomic ensemble for the temperature at $T = 50\ \mu$K is about tens of milliseconds [54], which is longer than the formation time required in our protocol by orders of magnitude. Hence, in the new basis spanned by $\{|G_1\rangle, |G_0\rangle, |R\rangle\}$, one can also introduce a Λ configuration for demonstrating the Rydberg superatom [55], giving rise to the single-atom Hamiltonian $\hat{\mathcal{H}}_1$ replaced by a new form $\hat{\mathcal{H}}_{\text{sa}}$,

$$\hat{\mathcal{H}}_{\text{sa}} = -\Delta(t)|R\rangle\langle R| + \left(\frac{\Omega(t)}{2}|R\rangle\langle G_1| + \frac{g}{2}|G_1\rangle\langle G_0| + \text{H.c.}\right). \tag{11}$$

Here $\hat{\mathcal{H}}_{\text{sa}}$ describes a Rydberg superatom interacting with light or microwave fields, serving as a starting point for a future consideration of steady dissipative entanglement between two long-range Λ Rydberg superatoms. Without loss of generality we will focus on the system with two individual atoms in the present work.

III. UNITARY DYNAMICS

A. Frequency modulation

In step (ii) we consider a reduced subspace with only two states $|11\rangle$ and $|rr\rangle$ [yellow box in Fig. 2(b)], in order to explore the frequency-modulated excitation dynamics. Intuitively when the reduced two-state system is driven via a continuous coupling, the system is a standard Rabi problem, revealing regular single-frequency oscillations (including excitation and deexcitation) of population between two states, where the oscillating frequency is exactly the same as the Rabi frequency. A striking difference arises once the driving is modulated to be time dependent dramatically modifying the Rabi behavior, leading to unexpected dynamics [56].

First we introduce a cosinoidal driving field $\Omega(t)$, denoted as

$$\Omega(t) = \Omega_0 \cos(\omega t), \tag{12}$$

focusing on the regime where the external modulation frequency ω is compatible with the characteristic frequency of the system. Such a time-dependent amplitude modulation for the peak Rabi frequency Ω_0 can be experimentally implemented via an acousto-optical modulator triggered via an electronic waveform generator controlling the acoustic profile, which can output shaped pulses [57]. Letting $\omega = 0$ leads to

$\Omega(t) = \Omega_0$, which stands for the case of a continuous pump that is the same as considered in previous works [19].

A brief introduction to the derivation of effective two-state Hamiltonian (6) can be understood in the subspace of $\{|11\rangle, |M\rangle, |rr\rangle\}$ with the singly excited collective state $|M\rangle = (|1r\rangle + |r1\rangle)/\sqrt{2}$. The original two-state Hamiltonian $\hat{\mathcal{H}}_{\rm uni}$ is

$$\hat{\mathcal{H}}_{\rm uni} = \frac{\Omega(t)}{\sqrt{2}}(|11\rangle\langle M|e^{i\Delta t} + |M\rangle\langle rr|e^{i\Delta t} + \text{H.c.}) + \hat{v}. \quad (13)$$

Working in a rotating-wave frame with respect to the rotational transformation $\hat{U} = e^{-iU_{\rm rr}|rr\rangle\langle rr|t}$, the above Hamiltonian can be reexpressed in a more concise form,

$$\hat{\mathcal{H}}'_{\rm eff,uni} = \frac{\Omega(t)^2}{2\Delta}(|11\rangle\langle rr| + |rr\rangle\langle 11|) - \frac{\Omega(t)^2}{\Delta}|M\rangle\langle M|, \quad (14)$$

where $U_{\rm rr} = 2\Delta$ and $\Delta \gg \Omega(t)/\sqrt{2}$ are assumed. Comparing (6) and (14), we ignore the second term $-\frac{\Omega(t)^2}{\Delta}|M\rangle\langle M|$ owing to its decoupling effect of state $|M\rangle$. The effective coupling strength $\frac{\Omega(t)^2}{2\Delta}$ between $|11\rangle$ and $|rr\rangle$ can be expressed as

$$\Omega_{\rm eff}(t) = \frac{\Omega_0^2}{4\Delta} + \frac{\Omega_0^2}{4\Delta}\cos(2\omega t), \quad (15)$$

which includes the base frequency component $\omega_0 = \frac{\Omega_0^2}{4\Delta}$ and the real-time modulated component $\omega_0\cos(2\omega t)$, giving to the peak amplitude belonging to $[0, 2\omega_0]$, as shown in the inset of Fig. 2(b). If $\omega \gg \omega_0$, the modulation term adds a fast high-frequency oscillation to the base frequency ω_0, whose effect can be averagely canceled within a sufficient time, i.e., $\int_0^\infty \omega_0\cos(2\omega t)dt = (\omega_0/2\omega)\sin(2\omega t)|_0^\infty \to 0$, arising a dominant base frequency ω_0 only; otherwise, the non-negligible modulated component will induce several modulated-frequency sidebands with separation ω to the central frequency ω_0, revealing complex multifrequency dynamical behavior.

B. Frequency spectrum analysis

By numerically solving the master equation $\dot{\rho}_{\rm uni} = i[\hat{\rho}_{\rm uni}, \hat{\mathcal{H}}_{\rm eff,uni}]$, we detect the observable quantity $P_{\rm rr}(t)$

$$P_{\rm rr}(t) = \langle rr|\hat{\rho}_{\rm uni}(t)|rr\rangle \quad (16)$$

for the time-dependent population probability on state $|rr\rangle$, where $\hat{\rho}_{\rm uni}(t)$ is the density matrix of the two-state subspace, as globally plotted in Fig. 3(a) versus time t and the relative modulation frequency ω/ω_0. Besides Fig. 3(b) describes a global view for the frequency spectrum of dynamics by implementing a Fourier transform $\mathcal{F}_{\rm rr}(\omega) = \int_{-\infty}^{+\infty} P_{\rm rr}(t)e^{-i\omega t}dt$. From Eq. (15) and Fig. 3(b) it is obvious that the presence of modulation ω can add frequency sidebands to the base frequency ω_0, which is also the characteristic frequency of the system, giving rise to the multiple frequencies $\omega_n = \omega_0 \pm n\omega$ with $n = 0, 1, 2, \ldots$, symmetrically located with respect to ω_0 [58]. As ω increases the dynamics become regular with one dominant base frequency ω_0 because a high-modulation-frequency ω will cause an average cancellation to the accumulated quantity by the frequency modulation $|(\omega_0/2\omega)\sin(2\omega t)_{t\to\infty}| \to 0$ as $\omega \gg \omega_0$. The inset of Fig. 2(b) comparably shows the Rabi oscillation behavior

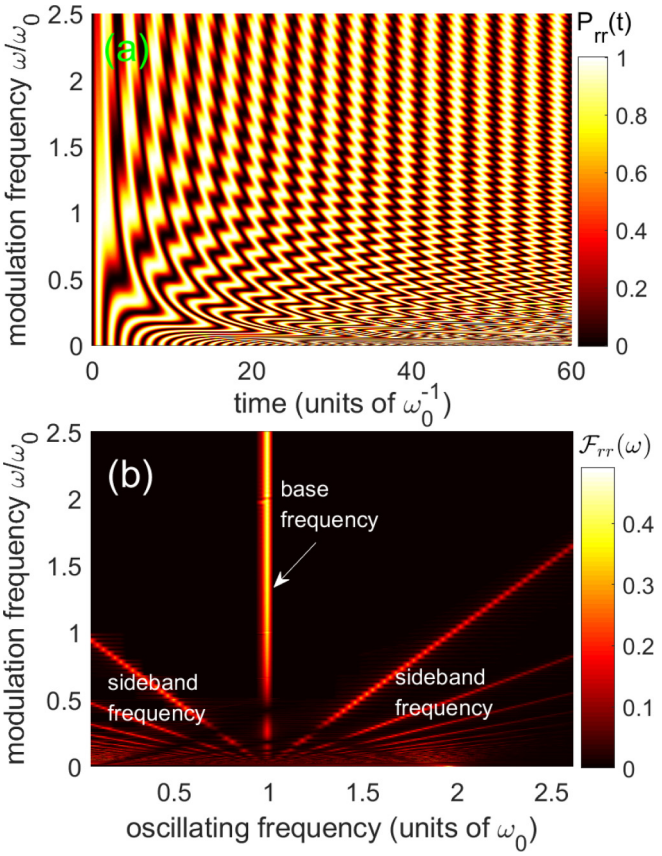

FIG. 3. Global output for (a) $P_{\rm rr}(t)$ and (b) $\mathcal{F}_{\rm rr}(\omega)$ versus the time $t \in (0, 60)$ and the relative modulation frequency $\omega/\omega_0 \in (0, 2.5)$. Parameters are $\Omega_0 = 57.6$, $U_{\rm rr} = 1658.88$, and $\Delta = 829.44$ and ω_0 (ω_0^{-1}) is the frequency (time) unit. Dissipation is ignored in calculating the unitary dynamics.

of $\Omega_{\rm eff}$ under weak (blue-solid) and strong (black-dashed) modulation frequencies.

As far as we know when the modulation is exactly an integral multiple of characteristic frequency ω_0, i.e., $\omega = n\omega_0$, the system exists as a dramatic frequency match, revealing unexpected behavior. To show this, we select $n = 0, 1, 2$ and represent the corresponding unitary dynamics and frequency spectrum in Figs. 4(a) and 4(b). Except for $\omega = 0$ that it reveals a complete single-frequency Rabi oscillation with frequency $2\omega_0$ [$\Omega_{\rm eff}(t) \equiv 2\omega_0$], the external frequency modulation $\omega[\neq 0]$ will give rise to sideband frequencies aside from the base frequency ω_0, with a tunable separation ω. The resulting unitary dynamics changes significantly by meeting different frequency matching conditions.

Comparing to the case of no modulation, it is observable that for $\omega = \omega_0$ (black-solid) the population dynamics $P_{\rm rr}(t)$ benefits from a sufficiently longer residence sustaining on the uppermost two-excitation state $|rr\rangle$, promising an efficient population dissipation onto the target state through spontaneous emission as long as the decay rate γ is suitable. Hence the frequency match offers an essential reason for the accelerated dissipative formation in step (iii). Furthermore, as ω increases, the system again tends to a single-frequency oscillation with the oscillating frequency ω_0, revealing regular modulated Rabi behavior. For example, if $\omega = 2\omega_0$

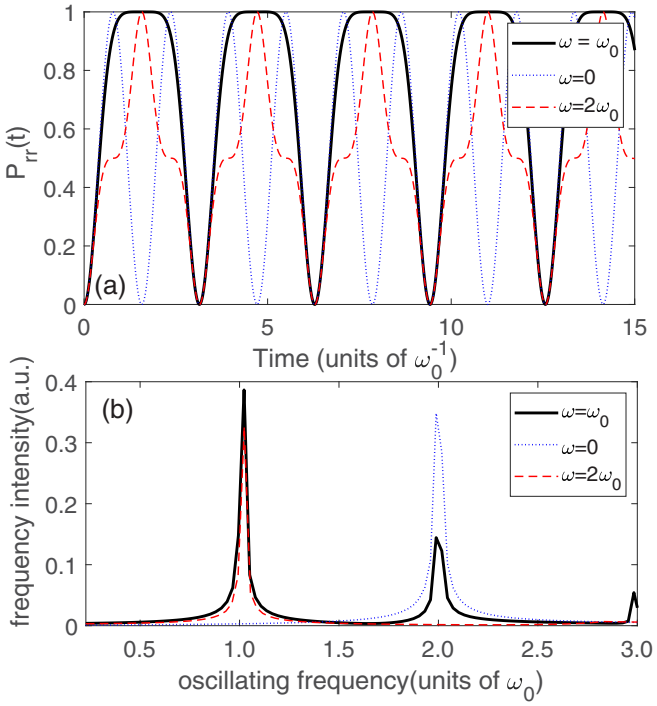

FIG. 4. (a), (b) Unitary dynamics $P_{rr}(t)$ and frequency spectrum $\mathcal{F}_{rr}(\omega)$ are comparably presented for $\omega = 0$ (blue-dotted), $\omega = \omega_0$ (black-solid), and $\omega = 2\omega_0$ (red-dashed) within a short time period of $\omega_0 t \in (0, 15)$. Other parameters are the same as adopted in Fig. 3.

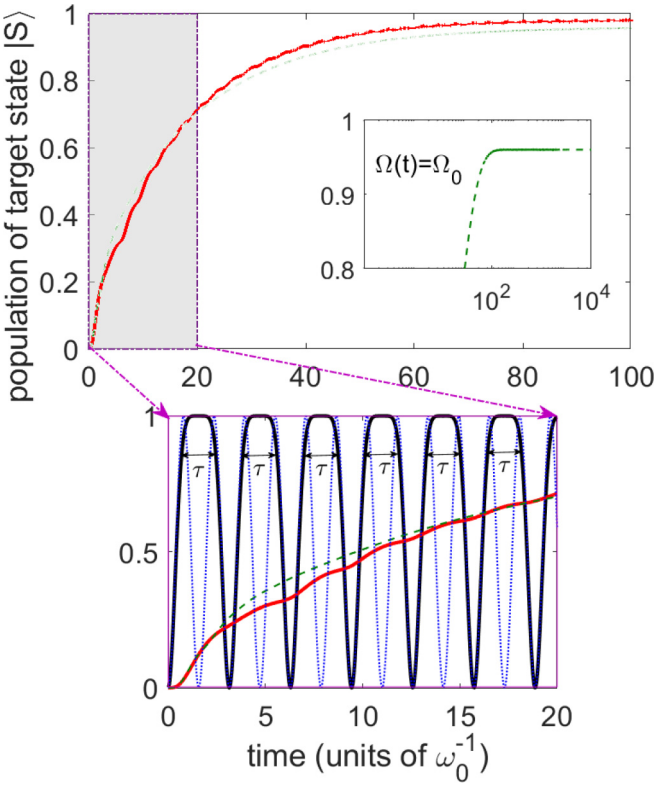

FIG. 5. Population of target entangled state $P_S(t)$ versus time t under the modulation frequency $\omega = \omega_0$ (red-solid) and $\omega = 0$ (green-dashed). A detailed plot of the relationship of the accumulated population in every duration τ on $|rr\rangle$ and unitary dynamics $P_{rr}(t)$ are comparably represented for time $t \in [0, 20]$ in the inset below. Inset inside shows an extensive plot by enlarging the time range to 10^4 where the final population for the case of no modulation $\Omega(t) = \Omega_0$ is kept to be a saturation ~0.96. Except the optimal parameters as discussed in Sec. III, here we choose $\gamma = 0.4$, $g = 0.85$ and set $P_{11}(t = 0) = 1.0$ at the initial time.

(red-dashed) $P_{rr}(t)$ suffers from a faster excitation and de-excitation processes without any stagnation on the upper state, leading to the population exchange in step (ii) between $|11\rangle \leftrightarrow |rr\rangle$ repeatedly. The resulting dissipative entanglement preparation is quite inefficient.

Based on the above analysis, we will adopt this optimal resonant modulation frequency $\omega = \omega_0$ for studying the accelerated entanglement preparation.

IV. FACILITATED ENTANGLEMENT FORMATION

The unitary dynamic evolution of the reduced two-state model can be guided to solve the complete master equation $\dot{\rho} = -i[\hat{\mathcal{H}}, \hat{\rho}] + \mathcal{L}[\hat{\rho}]$ for the entire system of a pair of three-level atoms, with the basic Hamiltonian $\hat{\mathcal{H}}$ [see Eq. (4)] as well as the Lindblad dissipation operators described by

$$\mathcal{L}[\hat{\rho}] = \sum_{i=1}^{4} \left[\hat{L}_i \hat{\rho} \hat{L}_i^\dagger - \frac{1}{2} (\hat{L}_i^\dagger \hat{L}_i \hat{\rho} + \hat{\rho} \hat{L}_i^\dagger \hat{L}_i) \right] \tag{17}$$

presenting the four spontaneous decay channels as shown in Fig. 2(a). According to the above discussion it is confirmed that $|S\rangle$ is an absolute unique steady state, arising the system ideally staying on that state as long as the evolution time is sufficient. However, due to the competition between unitary dynamics and the spontaneous dissipative process, the formation time can be endless, which is far beyond the detection time in a real implementation. Remember the typical time for entanglement formation basing on similar schemes is more than tens of milliseconds by using continuous driving with higher Rydberg levels $n > 100$ [59]. Here, with the help of a periodic amplitude modulation to the pump laser, it is observed that a clear entanglement facilitation can be confirmed, accompanied by a reduced detecting time ~$100/\omega_0$.

Figure 5 exhibits the real-time dynamics for population on target state $|S\rangle$, defined by $P_S(t) = \langle S|\hat{\rho}(t)|S\rangle$, with the modulation frequency $\omega = \omega_0$ (red-solid) or without modulation $\omega = 0$ (green-dashed). Clearly without periodical modulation, $P_S(t)$ represents a smoothly increasing curve but saturating towards 0.96 for $t \to \infty$; see the inset inside for an extensive range within $t \in [0, 10^4]/\omega_0$. However, with $\omega = \omega_0$, $P_S(t)$ exhibits a fast stepwise increase, even catching up with the case of $\omega = 0$ at $t = 14.3/\omega_0$, finally being stabilized to be as high as 0.98. That result benefits from an optimal frequency modulation, because for $\omega = 0$ it is impossible to reach 0.98 during the finite detection time. The reason accounting for this facilitation can be understood by finding longer durations τ in every oscillation period on state $|rr\rangle$ that is able to provide enough time of dissipation into the target state. As indicated clearly in the inset below, during each duration time τ [$P_{rr}(\tau) = 1.0$], $P_S(t)$ exhibits a dramatic enhancement especially at the initial time when the sufficient population can be exchanged between $|11\rangle$ and $|rr\rangle$.

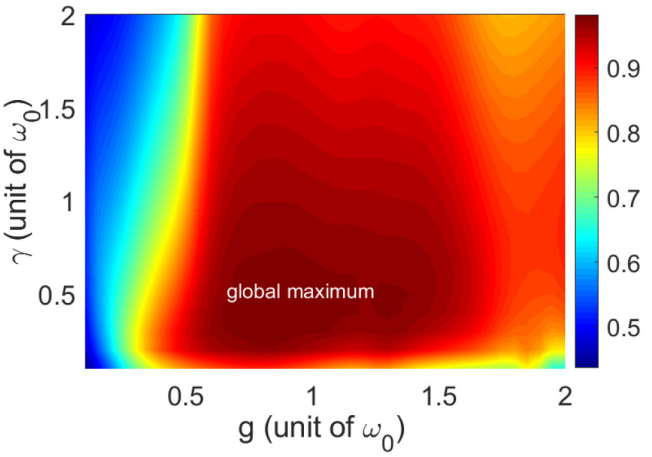

FIG. 6. Fidelity of final target entangled state $F_S[=P_S(t=100)]$ versus the simultaneous adjustments for microwave coupling g and spontaneous decay γ. A global maximum of F_S is denoted in the plot. Here ω_0 (ω_0^{-1}) is the frequency (time) unit.

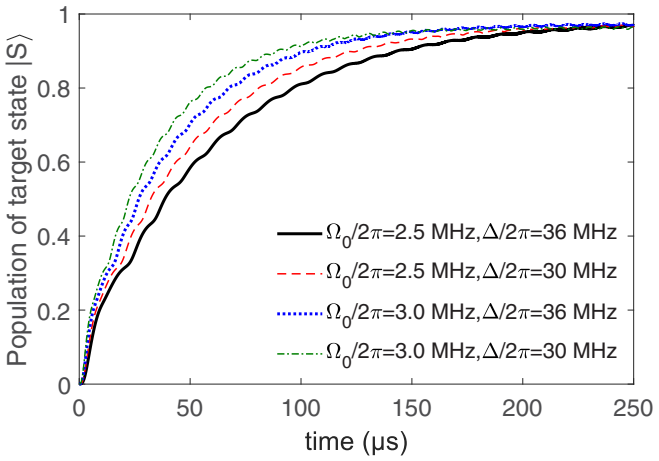

FIG. 7. Time-dependent population of the target state $P_S(t)$ versus $t(\mu s)$ for different Ω_0 and Δ values. Note that the conditions of $U_{rr}=2\Delta$ and $\omega=\omega_0$ are kept.

Also we stress the importance of competition among the unitary dynamics, spontaneous dissipation, and microwave coupling that leads to an accelerated entanglement formation. Therefore, we globally change the rates of dissipation γ and microwave coupling g in order to see the essential importance of frequency match to the fidelity of entanglement, characterized by the final fidelity $F_S=\langle S|\hat{\rho}(t=100/\omega_0)|S\rangle$. In Fig. 6, by varying γ and g within a same range $(0.1, 2.0)\omega_0$ there exists a global maximum region with $F_S\approx 0.98$ persistently, where the values of γ and g have a best matching. In contrast, beyond that range F_S reveals a considerable reduction, especially for a small g value arising a significantly poor transfer rate among $|11\rangle$, $|T\rangle$, $|00\rangle$ that cannot catch up with the (de)excitation and dissipation rates, leading to a very low entanglement production $F_S<0.5$. In other words, the realization of an accelerated entanglement formation needs an optimal modulation frequency ω implemented by an external pump laser, together with a perfect frequency consistence between the dissipative rate γ and microwave coupling strength g.

V. EXPERIMENTAL FEASIBILITY FOR FURTHER FACILITATION

In experiment the configuration like Fig. 2(a) can be implemented in two rubidium atoms where the hyperfine energy levels are $|1\rangle=|5s_{1/2},f=1,m=0\rangle$, $|0\rangle=|5s_{1/2},f=2,m=0\rangle$ that can be excited to the Rydberg state $|r\rangle=|100s\rangle$ via a two-photon transition mediated by, e.g., $|5p_{1/2}\rangle$. A practical calculation involving $|5p_{1/2}\rangle$ would be considered in the Appendix. Here the effective two-photon Rabi frequency is achieved to be a reasonable value $\Omega_0=2\pi\times 2.5$ MHz [27], with which the ground state $|1\rangle$ is coupled to the $|r\rangle$ by a big detuning $\Delta=2\pi\times 36$ MHz, giving rise to the characteristic frequency of system $\omega_0=\Omega_0^2/4\Delta=0.273$ MHz. In the design two atoms can be trapped separately with an interatomic distance $R=9.5$ μm for realizing a considerable vdW interaction $U_{rr}=2\pi\times 72$ MHz ($C_6/2\pi=5.3\times 10^{13}$ s$^{-1}\mu$m^6), driven by a periodically time-dependent laser beam $\Omega(t)$ with amplitude Ω_0 and modulation frequency $\omega=\omega_0=0.273$ MHz. Under an optimization for other frequency parameters we have $\gamma=2\pi\times 17$ kHz [60] and $g=2\pi\times 36.9$ kHz that enable a well coincidence with the unitary dynamics; the final fidelity for entangled state formation can attain as high as $F_S=0.981$ within a shortened operation time $T_S=366.3$ μs. From Fig. 6 these values γ and g can also be tunable in a global maximum region, e.g., $\gamma=2\pi\times 10$ kHz and $g=2\pi\times 34.8$ kHz, leading to $F_S=0.977$ within a same time T_S.

In addition, note that the optimal dynamics of $P_S(t)$ as displayed in Fig. 5 (red solid) reveals a stepwise-increasing behavior, dominantly decided by the increasing rate during the residence time τ on $|rr\rangle$ in the case of unitary dynamics. As a result an intuitive way for further facilitation to entanglement is increasing the effective coupling strength ω_0 between $|11\rangle$ and $|rr\rangle$, accelerating the accumulated rate of population on the target state during each residence. Figure 7 exhibits that, if Ω_0 increases or Δ decreases, leading to a stronger coupling value ω_0 for the excitation and deexcitation transitions during the laser pumping process, $P_S(t)$ can achieve a further accelerated growth, quickly saturating to a high-fidelity value $\sim$0.98 within a shorter time. It is confirmed that the case denoted by a green-dashed curve under $(\Omega_0,\Delta)=2\pi\times(3.0, 30)$ MHz shows a fastest speed to saturation. That fact provides an easy facilitation optimization in this scheme when other relevant frequency parameters are already suitable.

VI. ROBUST INSENSITIVITY OF SCHEME

A. Imperfect initialization

For exploring the relation of initial population distribution and the final fidelity of the target state we show the final fidelity under different initial population $P_{00}(0)$, $P_T(0)$, and $P_{11}(0)$, meeting the normalized condition $P_{11}(0)+P_T(0)+P_{00}(0)=1.0$. We need to point out that in plotting Fig. 8 we have calculated an average $\bar{F}_S$ value covering a duration of 100 μs for overcoming the slight population fluctuations

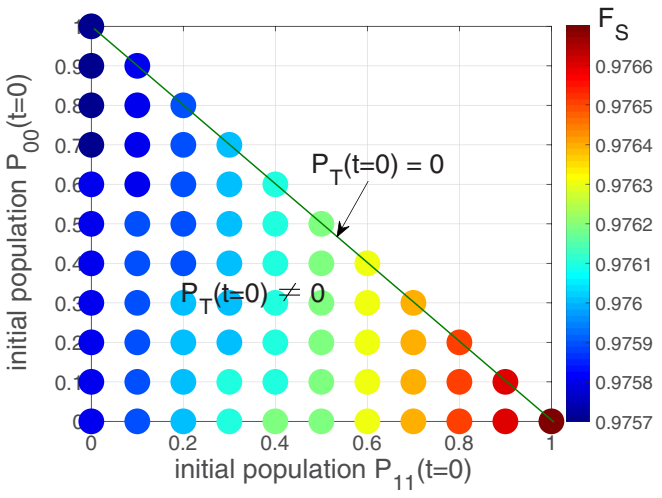

FIG. 8. Final fidelity $\bar{F}_S$ for a duration of $t \in [T_S - 100, T_S]\mu$s, versus the variation of initial population probability on ground states $|00\rangle$, $|T\rangle$, and $|11\rangle$, defined by $P_{00}(t=0)$, $P_T(t=0)$, and $P_{11}(t=0)$, satisfying the conserved normalization $P_{11}(0) + P_T(0) + P_{00}(0) = 1.0$. The target state $|S\rangle$ is initially unoccupied.

in its dynamics towards the saturation, which comes from a modified Rabi oscillation as in Fig. 5.

For atom initially occupying a determined state $|11\rangle$, i.e., $P_{11}(0) = 1.0$, the unitary dynamics in step (ii) between $|11\rangle$ and $|rr\rangle$ is straightforward, leading to a maximal average fidelity $\bar{F}_S \sim 0.9767$, as indicated by a dark red dot in Fig. 8. However, in an opposite case if atoms are entirely prepared in $|00\rangle$ that promises a fully indirect transfer to $|11\rangle$ mediated by $|T\rangle$, a very small decrease by an amplitude of $\Delta F_S \sim 0.001$ is observed for the average fidelity, strongly proving the robustness of fidelity insensitivity against this imperfect initialization. Otherwise, when the initial population is prepared imperfectly in a superposition state of $|00\rangle$, $|T\rangle$, $|11\rangle$ except the target state $|S\rangle$, a continuous coupling by the microwave field g among them would suffer from a persistent population transfer towards $|11\rangle$, causing a gradual varying of average fidelity between the former two cases. Intuitively, e.g., for a given P_{00} value, F_S continuously grows with the increase of P_{11}, which is directly connected to $|rr\rangle$. The above results again stress the flexibility and insensitivity of our scheme with respect to the system imperfect initialization, promising a feasible way for the generation of steady entanglement in the current experimental environment.

B. Variable vdW interactions

Consider in a real implementation the pair of atoms can be individually trapped in optical tweezers separated by a tunable distance R, enabled by changing the incidence angle of the formation beams. That achieves a large vdW interaction between the doubly excited Rydberg state $|rr\rangle$, well compensated by the detuning Δ, i.e., $2\Delta = U_{rr} = C_6/R^6$ (antiblockade). The current technique can control the distance R between the two atoms with a μm-scale accuracy; however, it is still possible to slightly vary the positions of the individual atoms under 1 μm during the entanglement formation of a few hundreds of μs, actually making the antiblockade condition unpreserved.

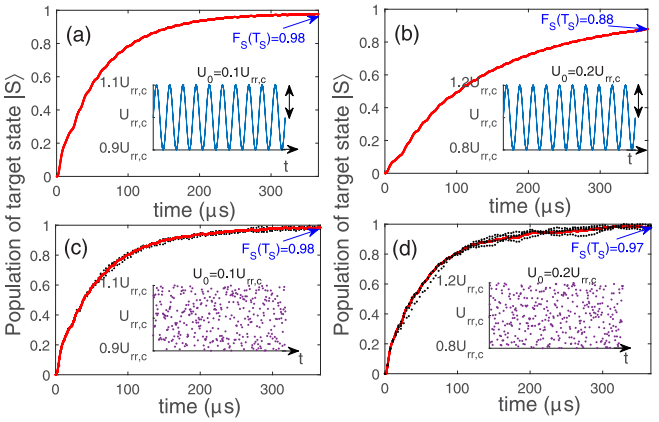

FIG. 9. Real time dependence of population $P_S(t)$ (red solid) on the target state $|S\rangle$ with variable vdW interactions $U_{rr}(t)$ realized by a slight change $\delta U(t)$ around its critical value $U_{rr,c}$. In case (i) $\delta U(t)$ shows a sinusoidal function with amplitudes (a) $U_0 = 0.1U_{rr,c}$ and (b) $U_0 = 0.2U_{rr,c}$. Turning to case (ii), $\delta U(t)$ is obtained randomly from $[-U_0, U_0]$ with (c) $U_0 = 0.1U_{rr,c}$ and (d) $U_0 = 0.2U_{rr,c}$.

To simulate the realistic dynamics under a variable interaction coming from the slight change of a two-atom distance, we add a time-dependent fluctuation $\delta U(t)$ to the critical value $U_{rr,c}$ by meeting $U_{rr}(t) = U_{rr,c} + \delta U(t)$. Here the exact antiblockade relation becomes $U_{rr,c} = 2\Delta$. For comparison the variation $\delta U(t)$ is assumed to take two different forms, as follows.

(i) A regular sinusoidal function

$$\delta U(t) = U_0 \sin(\omega_0' t) \tag{18}$$

with the frequency $\omega_0' = 200\omega_0$.

(ii) A stochastic function $\delta U(t)$ generated from

$$\delta U(t) \in [-U_0, U_0] \tag{19}$$

under small fluctuation amplitudes Figs. 9(a) and 9(c) $U_0 = 0.1U_{rr,c}$ and Figs. 9(b) and 9(d) $U_0 = 0.2U_{rr,c}$, corresponding to the slight change of relative positions around 0.32 μm and 0.64 μm, respectively. Based on the assumptions we calculate the population dynamics $F_S(t)$ with time (units of μs) on the target state $|S\rangle$, with respect to the time-dependent variation of interaction $\delta U(t)$ (see insets), as represented in Figs. 9(a)–9(d).

By carrying out a regular sinusoidal modification to the two-atom interaction as in case (i), the population of target state reveals a clear fall with the increase of modified amplitude U_0, which is verified by comparing Figs. 9(a) and 9(b) that the final fidelity $F_S(T_S)$ is only 0.88 when U_0 is increased to $0.2U_{rr,c}$. However, the real fluctuation of two-atom distance in experiment is unpredictable, leading to a better consideration of the stochastic change of vdW interaction between the two atoms; see Figs. 9(c) and 9(d), where random fluctuations $\delta U(t) \in [-U_0, U_0]$ are adopted. In the calculations we individually generate five sets of random data with (c) $U_0 = 0.1U_{rr,c}$ and (d) $U_0 = 0.2U_{rr,c}$, and the final target population labeled by red curves is achieved by a numerical fitting of all data (black dots). In fact, it is remarkable that the final fidelity of entangled state $|S\rangle$ has a surprising enhancement when the fluctuation of interactions is random in experiment, confirmed

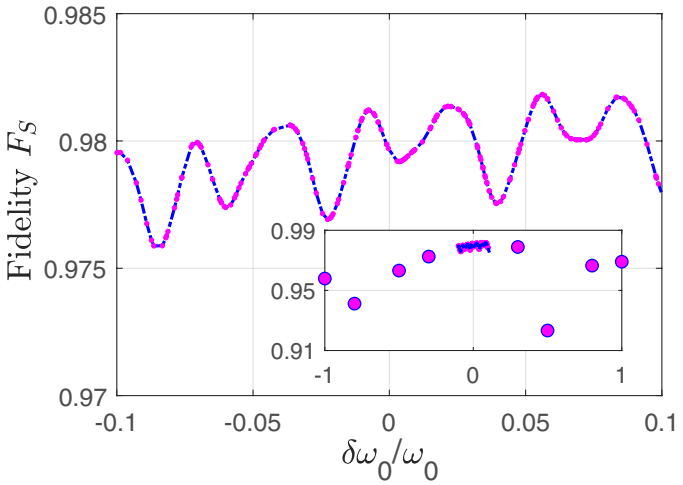

FIG. 10. Final fidelity F_S at $T_S = 366.3\ \mu$s versus a small variation of perturbation $\delta\omega_0$ to the periodic driving frequency ω_0, denoted by $\delta\omega_0/\omega_0 \in [-0.1, 0.1]$, i.e., the driving frequency changes from $0.9\omega_0$ to $1.1\omega_0$. Inset stands for an extensive range by modifying the range to $\delta\omega_0/\omega_0 \in [-1.0, 1.0]$.

by (d) where $F_s(T_s)$ persists to be as high as 0.97 [note that $F_s(T_s) = 0.88$ in (b)] by using $U_0 = 0.2U_{rr,c}$, promising a perfect insensitivity of robust entanglement generation to a slight change of two-atom distance (variable interactions) in a real implementation of our scheme.

C. Deviation of periodic driving frequency

To show the robustness of scheme we consider it works under small deviations $\delta\omega_0$ of the periodic driving from its base modification frequency ω_0, and verify a powerful insensitivity towards the variation of driving frequency as presented in Fig. 10. In the calculation by adding a small deviation $\pm 0.1\omega_0$ achieving the change of driving frequency from $0.9\omega_0$ to $1.1\omega_0$, the final fidelity F_S reveals a slight oscillation with the peak-peak oscillating amplitude smaller than 0.005, which offers a flexible way to determine the value of modification frequency in a realistic implementation. A bigger deviation of driving frequency extending to the range of $\delta\omega_0/\omega_0 \in [-1.0, 1.0]$ will cause a deep fall of the output fidelity accompanied by a stronger oscillation with amplitude one order of magnitude larger, see the inset of Fig. 10, again confirming the importance of using suitable driving frequencies that can facilitate not only the entanglement production efficiency but also a fast speed towards the final steady state.

VII. CONCLUSION

Originating from a pair of practical two four-level Λ-type Rydberg atoms, we show that when a periodically modulated pump laser is used one can achieve an accelerated formation of dissipative entangled steady state, arising an unprecedented facilitation mechanism that has never been considered in previous similar schemes. The merit of our scheme lies on the chosen of an external modulation frequency that exactly agrees with the characteristic frequency of the system, resulting in a dramatic modulation to the behavior of unitary dynamics in the optical pumping process. The modified Rabi oscillation behavior benefits from a longer residence time on the two-excitation Rydberg state, promising a fast decaying onto the target entangled state when the spontaneous emission rate and the microwave transferring rate are both tuned to be consistent at the same time. Under parameter optimization we successfully raise the fidelity to $\sim$0.98 with a formation time shorter than 400 μs. Comparably if no modulation is carried out it is found that the fidelity persists $\sim$0.96 for a sufficient time of tens of milliseconds, unenabling the realization of a higher entanglement within a limited detection time. Additionally we propose a way for further accelerating the convergence time by enhancing the effective coupling strength in the optical pump, and put forward to detailed discussions of the robust insensitivity of high fidelity against the imperfect preparation of initial states and the variable vdW interactions, as well as the deviation of modulated frequency in a real implementation.

For realizing a fast and high-fidelity dissipative steady entanglement, our proposal offers one step closer to this goal, simultaneously overcoming the obstacles from a complex energy-level structure (EIT approaches) or a long formation time (traditional Rydberg antiblockade approaches) in a number of previous works, which may provide different prospectives for experimentalists to create a maximal and deterministic steady entangled state via dissipation in interacting Rydberg systems.

ACKNOWLEDGMENTS

This work was supported by the NSFC under Grants No. 11474094, No. 11104076, and No. 11804308, by the China Postdoctoral Science Foundation Grant No. 2018T110735, by the Science and Technology Commission of Shanghai Municipality under Grant No. 18ZR1412800, and by the Academic Competence Funds for the outstanding doctoral students under Grant No. YBNLTS2019-023.

APPENDIX: UNITARY DYNAMICS OF FOUR-LEVEL ATOMS

In order to verify the feasibility of our simpler scheme in the text, we carry out a comparable calculation for the unitary dynamics between $|11\rangle$ and $|rr\rangle$ based on the original level structures [see Fig. 11(a)], adopted from two rubidium atoms with states $|1\rangle = |5s_{1/2}, f = 1, m = 0\rangle$, $|0\rangle = |5s_{1/2}, f = 2, m = 0\rangle$, $|p\rangle = |5p_{1/2}\rangle$, and $|r\rangle = |100s\rangle$. Rabi frequencies Ω_p and Ω_s are used for characterizing the optical couplings of $|1\rangle \leftrightarrows |p\rangle$ and $|p\rangle \leftrightarrows |r\rangle$ transitions. Here, the microwave coupling as well as all decays labeled by purple dashed curves in Fig. 11(a) are ignored. Remember in the frame of the effective system one has introduced two important parameters $\Omega(t) = \Omega_p\Omega_s/2\delta = \Omega_0\cos(\omega_0 t)$ and $\Delta(t) = (\Omega_p^2 - \Omega_s^2)/4\delta \approx$ const (compensated by $U_{\rm rr} = 2\Delta$) by which a high-fidelity entangled state $|S\rangle$ can be finally attained due to dissipation. Returning to the frame of an original atom-field interaction it requires the condition of $\delta = |\Delta_{1,2}| \gg \Omega_{p,s}$ and $\Delta_1 = -\Delta_2 = \delta$. For comparison here we adopt two sets of parameters Ω_p, Ω_s, δ, as represented in Figs. 11(b) and 11(c),

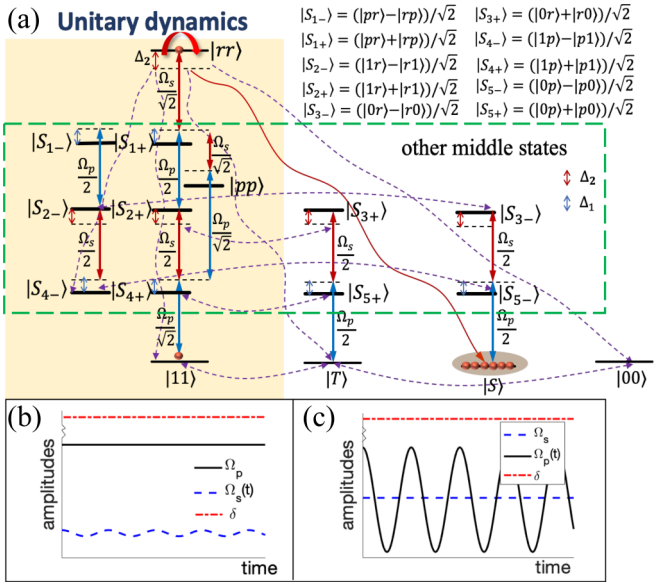

FIG. 11. Entire energy-level diagram of a pair of original four-level atoms. The unitary dynamics between $|11\rangle$ and $|rr\rangle$ as shown in the yellow box is mediated by two laser fields $\Omega_{p,s}$ and detunings $\Delta_{1,2}$. An effective five-level model that consists of states $\{|11\rangle, |T\rangle, |S\rangle, |00\rangle, |rr\rangle\}$ is finally obtained in the main text, by discarding all middle states for the off-resonant detunings $|\Delta_{1,2}| \gg \Omega_p, \Omega_s$. (b), (c) Two different designs of laser fields $\Omega_{p,s}$ and detuning $\delta = |\Delta_{1,2}|$, coinciding with the parameters $\Omega(t)$, $\Delta(t)$ in the effective two three-level atom system.

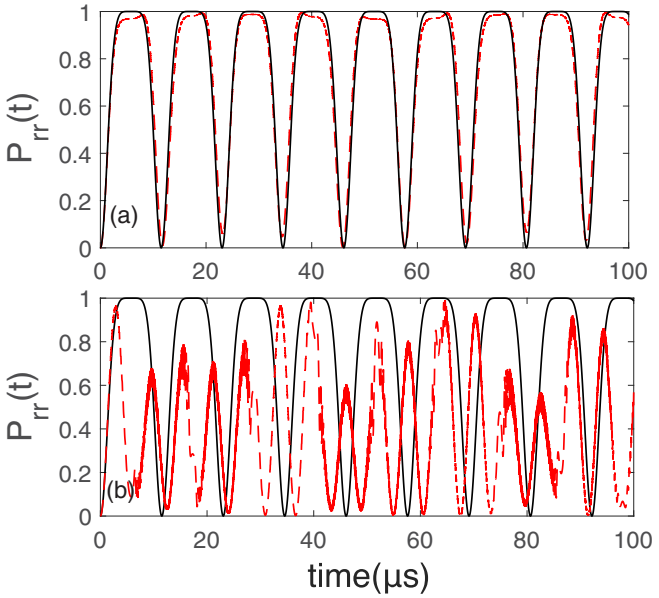

FIG. 12. Unitary dynamics of $P_{rr}(t)$ (red dashed) in an original pair of four-level atoms versus time (units of μs) under (a) a periodically modulated field $\Omega_s(t)$ and (b) a periodically modulated field $\Omega_p(t)$. Parameters are described in the text. The black solid curve stands for the unitary dynamics $P_{rr}(t)$ in the case of an effective system the same as presented in Fig. 4(a).

which are (b)

$$\Omega_s(t) = \Omega_{s0}\cos(\omega_0 t), \quad \Omega_p = \Omega_{p0} \tag{A1}$$

and (c)

$$\Omega_p(t) = \Omega_{p0}\cos(\omega_0 t), \quad \Omega_s = \Omega_{s0}, \tag{A2}$$

with $\Omega_{p0}/2\pi = 2.88$ GHz, $\Omega_{s0}/2\pi = 100$ MHz, $\delta/2\pi = 57.7$ GHz, and $\omega_0 = 0.273$ MHz. Note that $U_{rr} = 2\Delta$ is set to be preserved in the calculation no matter whether Δ is time dependent or not. Cases (b) and (c) only differ by a periodic modulation term $\cos(\omega_0 t)$ whether it is implemented on the weak field Ω_s or the strong field Ω_p.

By then we can calculate the original time-dependent unitary dynamics between the ground state $|11\rangle$ and the doubly excited state $|rr\rangle$ in an exact numerical way, as shown in Fig. 12, where the results from the effective system are plotted by black solid curves for contrast. Clearly when the coupling field Ω_s is modulated timely, a close consistence between the unitary dynamics of two models (original and effective) can be preserved, enabling a sufficient residence time on $|rr\rangle$ for the dissipation of population onto the target state. That fact could be understood by the well defined parameters $\Omega(t) = \Omega_s(t)\Omega_p/2\delta = (\Omega_{p0}\Omega_{s0}/2\delta)\cos(\omega_0 t)$ and $\Delta(t) = [\Omega_{p0}^2 - \Omega_{s0}^2\cos^2(\omega_0 t)]/4\delta \approx \Omega_{p0}^2/4\delta = \text{const}$ due to $\Omega_{p0} \gg \Omega_{s0}$. However, if the pump laser $\Omega_p(t)$ is modulated, $\Omega(t)$ is also well defined yet $\Delta(t) = [\Omega_{p0}^2\cos^2(\omega_0 t) - \Omega_{s0}^2]/4\delta \approx (\Omega_{p0}^2/4\delta)\cos^2(\omega_0 t)$ becomes a strongly oscillating function with amplitude $\Omega_{p0}^2/4\delta$ that cannot keep the requirement of a big detuning to the singly excited states as time evolves, arising a significant destruction for the unitary dynamics of $|11\rangle \leftrightarrows |rr\rangle$, since the effective system by discarding all singly excited states is unreasonable then. Therefore, we can robustly verify the validity of our simpler effective scheme compared with a real system in the experimental implementation.

[1] S. Diehl, A. Micheli, A. Kantian, B. Kraus, H. Büchler, and P. Zoller, Quantum states and phases in driven open quantum systems with cold atoms, Nat. Phys. **4**, 878 (2008).
[2] F. Verstraete. M. Wolf, and J. Cirac, Quantum computation and quantum-state engineering driven by dissipation, Nat. Phys. **5**, 633 (2009).
[3] J. Cho, S. Bose, and M. S. Kim, Optical Pumping into Many-Body Entanglement, Phys. Rev. Lett. **106**, 020504 (2011).
[4] M. J. Kastoryano, F. Reiter, and A. S. Sørensen, Dissipative Preparation of Entanglement in Optical Cavities, Phys. Rev. Lett. **106**, 090502 (2011).
[5] F. Reiter, M. Kastoryano, and A. Sørensen, Driving two atoms in an optical cavity into an entangled steady state using engineered decay, New. J. Phys. **14**, 053022 (2012).
[6] E. G. Dalla Torre, J. Otterbach, E. Demler, V. Vuletic, and M. D. Lukin, Dissipative Preparation of Spin Squeezed Atomic Ensembles in a Steady State, Phys. Rev. Lett. **110**, 120402 (2013).

[7] F. Reiter, D. Reeb, and A. S. Sørensen, Scalable Dissipative Preparation of Many-Body Entanglement, Phys. Rev. Lett. **117**, 040501 (2016).

[8] Z.-P. Cian, G. Zhu, S.-K. Chu, A. Seif, W. DeGottardi, L. Jiang, and M. Hafezi, Photon Pair Condensation by Engineered Dissipation, Phys. Rev. Lett. **123**, 063602 (2019).

[9] J. Barreiro, M. Müller, P. Schindler, D. Nigg, T. Monz, M. Chwalla, M. Hennrich, C. Roos, P. Zoller, and R. Blatt, An open-system quantum simulator with trapped ions, Nature (London) **470**, 486 (2011).

[10] Y. Lin, J. Gaebler, F. Reiter, T. Tan, R. Bowler, A. Sørensen, D. Leibfried, and D. Wineland, Dissipative production of a maximally entangled steady state of two quantum bits, Nature (London) **504**, 415 (2013).

[11] S. Shankar, M. Hatridge, Z. Leghtas, K. Sliwa, A. Narla, U. Vool, S. M. Girvin, L. Frunzio, M. Mirrahimi, and M. Devoret, Autonomously stabilized entanglement between two superconducting quantum bits, Nature (London) **504**, 419 (2013).

[12] M. E. Kimchi-Schwartz, L. Martin, E. Flurin, C. Aron, M. Kulkarni, H. E. Tureci, and I. Siddiqi, Stabilizing Entanglement via Symmetry-Selective Bath Engineering in Superconducting Qubits, Phys. Rev. Lett. **116**, 240503 (2016).

[13] H. Krauter, C. A. Muschik, K. Jensen, W. Wasilewski, J. M. Petersen, J. I. Cirac, and E. S. Polzik, Entanglement Generated by Dissipation and Steady State Entanglement of Two Macroscopic Objects, Phys. Rev. Lett. **107**, 080503 (2011).

[14] A. W. Carr and M. Saffman, Preparation of Entangled and Antiferromagnetic States by Dissipative Rydberg Pumping, Phys. Rev. Lett. **111**, 033607 (2013).

[15] D. D. B. Rao and K. Mølmer, Dark Entangled Steady States of Interacting Rydberg Atoms, Phys. Rev. Lett. **111**, 033606 (2013).

[16] H. Weimer, M. Müller, I. Lesanovsky, P. Zoller, and H. Büchler, A Rydberg quantum simulator, Nat. Phys. **6**, 382 (2010).

[17] M. Saffman, Quantum computing with atomic qubits and Rydberg interactions: progress and challenges, J. Phys. B: At., Mol., Opt. Phys. **49**, 202001 (2016).

[18] X.-Q. Shao, J.-B. You, T.-Y. Zheng, C. H. Oh, and S. Zhang, Stationary three-dimensional entanglement via dissipative Rydberg pumping, Phys. Rev. A **89**, 052313 (2014).

[19] S.-L. Su, Q. Guo, H.-F. Wang, and S. Zhang, Simplified scheme for entanglement preparation with Rydberg pumping via dissipation, Phys. Rev. A **92**, 022328 (2015).

[20] X. Chen, G.-W. Lin, H. Xie, X. Shang, M.-Y. Ye, and X.-M. Lin, Fast creation of a three-atom singlet state with a dissipative mechanism and Rydberg blockade, Phys. Rev. A **98**, 042335 (2018).

[21] Y.-H. Chen, Z.-C. Shi, J. Song, Y. Xia, and S.-B. Zheng, Accelerated and noise-resistant generation of high-fidelity steady-state entanglement with Rydberg atoms, Phys. Rev. A **97**, 032328 (2018).

[22] Y.-H. Chen, W. Qin, and F. Nori, Fast and high-fidelity generation of steady-state entanglement using pulse modulation and parametric amplification, Phys. Rev. A **100**, 012339 (2019).

[23] L.-T. Shen, X.-Y. Chen, Z.-B. Yang, H.-Z. Wu, and S.-B. Zheng, Steady-state entanglement for distant atoms by dissipation in coupled cavities, Phys. Rev. A **84**, 064302 (2011).

[24] S.-L. Su, X.-Q. Shao, H.-F. Wang, and S. Zhang, Scheme for entanglement generation in an atom-cavity system via dissipation, Phys. Rev. A **90**, 054302 (2014).

[25] X.-Q. Shao, T.-Y. Zheng, C. H. Oh, and S. Zhang, Dissipation creation of three-dimensional entangled state in an optical cavity via spontaneous emission, Phys. Rev. A **89**, 012319 (2014).

[26] X. Q. Zhao, Z. H. Wang, H. D. Liu, and X. X. Yi, Dissipative preparation of a tripartite singlet state in coupled arrays of cavities via quantum feedback control, Phys. Rev. A **94**, 032307 (2016).

[27] X. Q. Shao, J. H. Wu, X. X. Yi, and G.-L. Long, Dissipative preparation of steady Greenberger-Horne-Zeilinger states for Rydberg atoms with quantum Zeno dynamics, Phys. Rev. A **96**, 062315 (2017).

[28] S. Denisov, L. Morales-Molina, S. Flach, and P. Hänggi, Periodically driven quantum ratchets: Symmetries and resonances, Phys. Rev. A **75**, 063424 (2007).

[29] P. M. Poggi, F. J. Arranz, R. M. Benito, F. Borondo, and D. A. Wisniacki, Maximum population transfer in a periodically driven quantum system, Phys. Rev. A **90**, 062108 (2014).

[30] V. I. Yudin, A. V. Taichenachev, and M. Y. Basalaev, Dynamic steady state of periodically driven quantum systems, Phys. Rev. A **93**, 013820 (2016).

[31] B. Baran and T. Domański, Quasiparticles of a periodically driven quantum dot coupled between superconducting and normal leads, Phys. Rev. B **100**, 085414 (2019).

[32] G. S. Agarwal and W. Harshawardhan, Realization of trapping in a two-level system with frequency-modulated fields, Phys. Rev. A **50**, R4465(R) (1994).

[33] M. W. Noel, W. M. Griffith, and T. F. Gallagher, Frequency-modulated excitation of a two-level atom, Phys. Rev. A **58**, 2265 (1998).

[34] D. Li and S. Xiao, Rapid population transfer of a two-level system by a polychromatic driving field, Sci. Rep. **9**, 9023 (2019).

[35] M. Macovei and C. H. Keitel, Quantum dynamics of a two-level emitter with a modulated transition frequency, Phys. Rev. A **90**, 043838 (2014).

[36] N.-B. Manson, C. Wei, and J. P. D. Martin, Response of a Two-Level System Driven by Two Strong Fields, Phys. Rev. Lett. **76**, 3943 (1996).

[37] F. M. Gambetta, F. Carollo, M. Marcuzzi, J. P. Garrahan, and I. Lesanovsky, Discrete Time Crystals in the Absence of Manifest Symmetries or Disorder in Open Quantum Systems, Phys. Rev. Lett. **122**, 015701 (2019).

[38] W. C. Yu, J. Tangpanitanon, A. W. Glaetzle, D. Jaksch, and D. G. Angelakis, Discrete time crystal in globally driven interacting quantum systems without disorder, Phys. Rev. A **99**, 033618 (2019).

[39] J. Eisert, M. Friesdorf, and C. Gogolin, Quantum many-body systems out of equilibrium, Nat. Phys. **11**, 124 (2015).

[40] K. Brandner and U. Seifert, Periodic thermodynamics of open quantum systems, Phys. Rev. E **93**, 062134 (2016).

[41] V. Reimer, K. G. L. Pedersen, N. Tanger, M. Pletyukhov, and V. Gritsev, Nonadiabatic effects in periodically driven dissipative open quantum systems, Phys. Rev. A **97**, 043851 (2018).

[42] D. A. Abanin, W. De Roeck, and F. Huveneers, Exponentially Slow Heating in Periodically Driven Many-Body Systems, Phys. Rev. Lett. **115**, 256803 (2015).

[43] Y. Ge and M. Rigol, Topological phase transitions in finite-size periodically driven translationally invariant systems, Phys. Rev. A **96**, 023610 (2017).

[44] O. Shtanko and R. Movassagh, Stability of Periodically Driven Topological Phases against Disorder, Phys. Rev. Lett. **121**, 126803 (2018).

[45] E. B. Aranas, M. J. Akram, D. Malz, and T. S. Monteiro, Quantum noise spectra for periodically driven cavity optomechanics, Phys. Rev. A **96**, 063836 (2017).

[46] S. Basak, Y. Chougale, and R. Nath, Periodically Driven Array of Single Rydberg Atoms, Phys. Rev. Lett. **120**, 123204 (2018).

[47] A. L. Gramajo, D. Domínguez, and M. J. Sánchez, Amplitude tuning of steady-state entanglement in strongly driven coupled qubits, Phys. Rev. A **98**, 042337 (2018).

[48] Y. Miroshnychenko, A. Gaëtan, C. Evellin, P. Grangier, D. Comparat, P. Pillet, T. Wilk, and A. Browaeys, Coherent excitation of a single atom to a Rydberg state, Phys. Rev. A **82**, 013405 (2010).

[49] E. Brion, L. Pedersen, and K. Mølmer, Adiabatic elimination in a lambda system, J. Phys. A: Math. Theor. **40**, 1033 (2007).

[50] M. M. Müller, M. Murphy, S. Montangero, T. Calarco, P. Grangier, and A. Browaeys, Implementation of an experimentally feasible controlled-phase gate on two blockaded Rydberg atoms, Phys. Rev. A **89**, 032334 (2014).

[51] Y.-H. Chen, Z.-C. Shi, J. Song, Y. Xia, and S.-B. Zheng, Coherent control in quantum open systems: An approach for accelerating dissipation-based quantum state generation, Phys. Rev. A **96**, 043853 (2017).

[52] I. I. Beterov, M. Saffman, E. A. Yakshina, V. P. Zhukov, D. B. Tretyakov, V. M. Entin, I. I. Ryabtsev, C. W. Mansell, C. MacCormick, S. Bergamini, and M. P. Fedoruk, Quantum gates in mesoscopic atomic ensembles based on adiabatic passage and Rydberg blockade, Phys. Rev. A **88**, 010303(R) (2013).

[53] M. Ebert, M. Kwon, T. G. Walker, and M. Saffman, Coherence and Rydberg Blockade of Atomic Ensemble Qubits, Phys. Rev. Lett. **115**, 093601 (2015).

[54] M. Saffman and T. G. Walker, Analysis of a quantum logic device based on dipole-dipole interactions of optically trapped Rydberg atoms, Phys. Rev. A **72**, 022347 (2005).

[55] P. Z. Zhao, X. Wu, T. H. Xing, G. F. Xu, and D. M. Tong, Nonadiabatic holonomic quantum computation with Rydberg superatoms, Phys. Rev. A **98**, 032313 (2018).

[56] R. Glenn, M. E. Limes, B. Pankovich, B. Saam, and M. E. Raikh, Magnetic resonance in slowly modulated longitudinal field: Modified shape of the Rabi oscillations, Phys. Rev. B **87**, 155128 (2013).

[57] A. Weiner, Ultrafast optical pulse shaping: A tutorial review, Opt. Commun. **284**, 3669 (2011).

[58] Z. Ficek, J. Seke, A. V. Soldatov, and G. Adam, Fluorescence spectrum of a two-level atom driven by a multiple modulated field, Phys. Rev. A **64**, 013813 (2001).

[59] X. Chen, H. Xie, G.-W. Lin, X. Shang, M.-Y. Ye, and X.-M. Lin, Dissipative generation of a steady three-atom singlet state based on Rydberg pumping, Phys. Rev. A **96**, 042308 (2017).

[60] I. I. Beterov, I. I. Ryabtsev, D. B. Tretyakov, and V. M. Ent, Quasiclassical calculations of blackbody-radiation-induced depopulation rates and effective lifetimes of Rydberg nS, nP, and nD alkali-metal atoms with $n \leqslant 80$, Phys. Rev. A **79**, 052504 (2009).